

Numerical simulation of active structural-acoustic control for a fluid-loaded, spherical shell

Christopher E. Ruckman

Structural Acoustics and Hydroacoustics Research Branch, Carderock Division, Naval Surface Warfare Center, Bethesda, Maryland 20084-5000

Chris R. Fuller

Vibration and Acoustics Laboratories, Virginia Polytechnic Institute and State University, Blacksburg, Virginia 24061

(Received 10 November 1992; revised 4 November 1993; accepted 14 June 1994)

Numerical methods are used to investigate active structural-acoustic control, a noise control technique in which oscillating force inputs are applied directly on a flexible structure to control its acoustic behavior. The goal is to control acoustic radiation from a thin-walled shell submerged in a dense fluid and subjected to a persistent, pure-tone disturbance. For generality the fully coupled responses are found numerically, in this case using the computer program that combines finite-element and boundary-element techniques. A feedforward control approach uses linear quadratic optimal control theory to minimize the total radiated power. Results are given for a thin-walled spherical shell, and are compared to analytical results. The numerical solution is shown to be suitably accurate in predicting the radiated power, the control forces, and the residual responses as compared to the analytical solution. A relatively small number of control forces can achieve global reductions in acoustic radiation at low frequencies ($k_0 a < 1.7$). A single point-force actuator reduces the radiated power due to a point-force excitation by up to 20 dB at resonance frequencies; between resonance frequencies, more actuators are required because of modal spillover. With multiple control forces, radiation can be reduced by 6–20 dB over the frequency range $0 < k_0 a < 1.7$.

PACS numbers: 43.40.Vn, 43.40.Rj

INTRODUCTION

The concept of active structural-acoustic control (ASAC) involves controlling the acoustic response of a fluid-structure system by applying oscillating force inputs directly to the structure. Recent theoretical and experimental studies have used ASAC to control radiation from one- and two-dimensional structures including beams, plates, and submerged plates; similar techniques were used to control noise transmitted through flat plates or into infinite cylindrical shells.^{1–6} The concept is similar to active vibration control since the actuators are vibrational inputs applied directly on a flexible structure, but the goal of reducing acoustic response often differs from the goal of reducing a purely structural response. ASAC also differs from active noise cancellation (ANC), since ASAC applies vibrational inputs to the structure itself rather than exciting the acoustic medium with loudspeakers.⁷ For structure-borne noise, ASAC can often produce widespread far-field reductions with a relatively few actuators as compared to ANC. Also, because vibrational inputs tend to be more compact than loudspeakers, ASAC can be used in certain situations where ANC is impractical.

Submerged shells and other fluid-loaded structures are of significant practical interest, but they also represent a fundamental departure from existing work. Most nonexperimental studies of ASAC have used analytical approaches to obtain the required structural-acoustic quantities. However, for a general, three-dimensional, fluid-loaded shell no such analytical expressions exist. In the present research, dynamic

responses are obtained using the computer program NASHUA.⁸ NASHUA uses the finite-element method to compute structural quantities, and a boundary-element formulation to solve for the fully coupled structural-acoustic response. A similar study is given by Molo and Bernhard,⁹ who used the indirect boundary-element method to formulate active noise cancellation systems for both interior and exterior noise fields. Another related study is by Cunefare and Koopman,¹⁰ which uses a boundary-element approach to examine three-dimensional exterior problems. The main differences from the present work are that the system includes an elastic structure with full fluid-structure coupling, and the control actuators are vibrational inputs rather than acoustic sources.

There are two significant benefits to using an approach based on finite elements/boundary elements. First, altering model geometries involves minimal effort because the boundary-element formulation does not require discretization of the ambient fluid. Second, the approach can treat nearly any structure amenable to finite-element modeling, making it an excellent companion for theoretical and experimental studies of submerged shells.

The present report is an extension to Ref. 11, which outlines some preliminary results obtained by applying these techniques to a thin, spherical shell with fluid loading. A more comprehensive set of results is given, with more emphasis on showing agreement between numerical and analytical results. The aim is to gain confidence in the use of

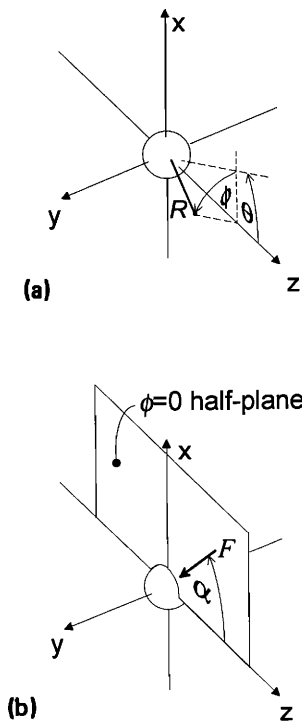


FIG. 1. Coordinate systems for defining (a) sensor locations in the far field, and (b) force locations on the shell. Control forces are restricted to lie within the $\phi=0$ half-plane, thus force locations may be defined by a single angular coordinate α .

numerical techniques for more complex situations.

The following work analyzes steady-state, single-frequency forcing functions. The control algorithm used is a feedforward method which requires *a priori* knowledge of the frequency content and location of the disturbance force. After specifying the number and locations of the control actuators, linear quadratic optimal control theory is used to solve for the complex control forces that minimize a quadratic cost function.

I. THEORETICAL BACKGROUND

This section describes the analytical and numerical models of the structure–fluid system and the feedforward control approach used to find control forces and phases.

A. Analytical and numerical modeling of spherical shell

Figure 1(a) defines the coordinate systems used for the thin-walled spherical shell. The global z axis is defined as the axis along which the disturbance force acts. Far-field locations are defined in global spherical coordinates (R, θ, ϕ) , where R is the radial distance, θ the latitudinal angle measured from the global z axis, and ϕ the longitudinal angle measured from the x - z plane. The structure is completely submerged in a dense fluid, with material properties chosen to resemble a steel shell in water. The ratio of shell thickness to radius is 0.01, and the shell radius is $a=1$ m. Frequencies up to $k_0a=1.7$ are examined, where k_0 is the acoustic wave number; this frequency range includes the resonance frequencies of several low-order modes.

To simplify the problem, a restricted set of forcing functions is considered for disturbance and control forces. The forces are concentrated loads (point forces) normal to the shell surface, and are applied only in the $\phi=0$ plane as shown in Fig. 1(b). Force locations are specified by a single angle α . The disturbance is always a single point-force applied to $\alpha=0$. The total far-field response is therefore either axisymmetric (if a single control force is applied at $\theta=\pi$), or symmetric about the $\phi=0$ plane (if a control force is applied off the z axis.)

Multiforce responses can be found by combining the axisymmetric responses due to each of the individual forces using superposition, even if their combined response is not axisymmetric. Given the restrictions on force locations described above, the coordinate transformation used to find radiation and shell vibration due to any individual force is a simple rotation whose effective rotation angle can be found from the following relation:

$$\cos \theta_{\text{eff}} = (\cos^2 \theta + \sin^2 \theta \sin^2 \phi)^{1/2} \times \cos \left[\alpha + \tan^{-1} \left(\frac{\sin \theta \sin \phi}{\cos \theta} \right) \right]. \quad (1)$$

The analytical model for a thin-walled, fluid-loaded, spherical shell with a radially directed, persistent, point force is due to Junger and Feit.² The model includes membrane stresses but ignores bending stresses, and is therefore limited to low frequencies. The far-field pressure due to a force b_i applied on along the z axis is

$$P(R, \theta, b_i) = \sum_{n=0}^{\infty} b_i \Gamma_n(R) \mathbf{P}_n(\cos \theta), \quad (2)$$

where \mathbf{P}_n is the Legendre polynomial of order n , and

$$\Gamma_n(R) = \frac{2n+1}{4\pi a^2} \left(\frac{\rho c}{k_a R} \right) \frac{(-\sqrt{-1})^n}{(Z_n + z_n) h'(k_a a)}. \quad (3)$$

The symbols ρ and c represent the fluid density and acoustic velocity, and h is the spherical Hankel function. The modal acoustic impedance is

$$z_n = j \rho c \frac{h_n(ka)}{h'_n(ka)}, \quad (4)$$

and the modal structural impedance is

$$Z_n = -j \frac{h}{a} \rho_s c_p \frac{\{\Omega^2 - (\Omega_n^{(1)})^2\} \{\Omega^2 - (\Omega_n^{(2)})^2\}}{\Omega^3 - \Omega(n^2 + n - 1 - \nu)}, \quad (5)$$

where $\Omega_n^{(1)}$ and $\Omega_n^{(2)}$ are the two *in vacuo* natural frequencies associated with the roots of

$$\Omega^4 - (1 + 3\nu + \lambda^n) \Omega^2 + (\lambda^n - 2)(1 - \nu^2). \quad (6)$$

For numerical modeling, the computer program NASHUA is used to compute both structural responses and far-field acoustic responses. NASHUA uses the finite-element program NASTRAN to compute mass, damping, and stiffness matrices for the structure. These are used with a discretized form of the Helmholtz surface integral equation to obtain the response of the fully coupled response of the fluid-structure system. Such techniques are well known and are not detailed

here; the interested reader is referred to Ref. 8.

While NASHUA is capable of fully three-dimensional modeling, only axisymmetric models are used here to simplify analysis and reduce computing costs. The finite-element portion of the NASHUA model uses axisymmetric cone elements that include both bending and membrane stresses. The structural mesh contains 129 grid circles. Since NASTRAN does not allow grid circles with zero radius, the poles at $\theta=0$ and $\theta=\pi$ are actually "pinholes" or grid circles of radius $0.001a$. To approximate a point force, a ring force is applied on one of the small-radius grid circles. This approximation casts some doubt on the validity of the model at high frequencies. However, as described below, the agreement between analytical and numerical results is sufficient for the problem at hand.

B. Feedforward control approach

The control approach taken here is a single-frequency, steady-state, feedforward approach based on linear quadratic optimal control theory.^{2,3,9} Consider a spherical shell subjected to a total of N_d coherent, persistent, time-harmonic disturbance forces. The disturbance response P_d , also known as the primary response, is defined as the far-field pressure due to these disturbance forces. Here the disturbance response is axisymmetric to make the development more clear, but any type of disturbance could be used. Suppose the i th disturbance force has strength s_i , and would cause far-field pressure distribution $A_i(\theta)$ if acting alone. Assuming linearity, the disturbance response can be written as a linear sum of the individual disturbance responses:

$$P_d(\theta) = \sum_{i=1}^{N_d} A_i(\theta) s_i. \quad (7)$$

Suppose a total of N control forces are now applied to control the disturbance response, where the i th control force has strength b_i . The control response \hat{P} , also known as the secondary response, is defined as the far-field pressure due to only the control forces. Furthermore, suppose that both the control response and the disturbance response must be symmetric about the same axis so that their sum is axisymmetric. Thus the control response $\hat{P}(\theta)$ is a linear sum of the individual control responses $X_i(\theta)$:

$$\hat{P}(\theta) = \sum_{i=1}^N X_i(\theta) b_i. \quad (8)$$

The total response is the sum of the disturbance response plus the control response.

Now define a quadratic cost function χ^2 as a weighted integral of squared magnitude of the total response over the entire far field which, because of symmetry, is a single integral:

$$\chi^2 = \int_0^\pi w(\theta) |P_d(\theta) + \hat{P}(\theta)|^2 d\theta, \quad (9)$$

where $w(x)$ is a weighting function that can be chosen to give physical significance to χ^2 if desired. The feedforward control problem can be restated as an unconstrained qua-

dratic minimization, i.e., seek a set of control forces b_i to minimize χ^2 . Since the total radiated power is

$$\Pi = \int_0^\pi \frac{\pi R^2 \sin \theta}{\rho c} |p(\theta)|^2 d\theta, \quad (10)$$

a cost function equal to the total radiated power can be found by setting

$$w(\theta) = (\pi R^2 / \rho c) \sin \theta. \quad (11)$$

The set of control forces that minimizes χ^2 is the set of control forces for which $\partial\Pi/\partial b_i$ vanishes for each of the N control forces b_i . This requirement produces an $N \times N$ system of complex-valued, simultaneous equations, the so-called normal equations, which have as their solution the control forces b_i . The coefficients of the normal equations can be generated in either of two ways, depending on whether $P_c(\theta)$ and $\hat{P}(\theta)$ are given as continuous functions of θ or as discretized functions defined only at discrete values of θ . With continuous expressions for the variables, the integration in Eq. (6) can be performed in closed form. On the other hand, if the variables are defined only at discrete locations, it is necessary to generate discrete (analytical or numerical) transfer functions and integrate Eq. (6) numerically. These two methods are outlined below.

Note that each of the variables A_i and X_i from Eqs. (4) and (5) is merely a transfer function between a unit force somewhere on the structure and the far-field pressure distribution. In the present context these transfer functions are found using either NASHUA or an analytical solution. However, for purposes of simulation they could be obtained from any source such as experimental data or other numerical solutions. Note also that Eq. (6) contains a line integral for a one-dimensional system but could be extended to an integral over an area or through a volume.

1. Obtaining the normal equations from continuous variables

When an analytical solution is available, the problem can be formulated in terms of continuous functions of far-field location θ . It is possible to integrate Eq. (6) in closed form, evaluate the coefficients of the normal equations, and solve for the required control forces. Suppose the control forces and disturbance forces are written in vector form so that

$$B = \{b_1 \quad b_2 \quad \cdots \quad b_N\}^T \quad (12)$$

and

$$S = \{s_1 \quad s_2 \quad \cdots \quad s_N\}^T.$$

Now write the disturbance response as $P_d(\theta) = AS$ and the control response as $\hat{P}(\theta) = XB$, where A and X are row vectors containing the continuous variables $A_i(\theta)$ and $X_i(\theta)$ from Eqs. (4) and (5), respectively. For instance, the form of X is

$$X = \{X_1(\theta) \quad X_2(\theta) \quad \cdots \quad X_N(\theta)\}, \quad (13)$$

and likewise for A . After some algebra, the cost function from Eq. (6) becomes

$$\begin{aligned} \chi^2 = & \int_0^\pi B^H X^H X B w(\theta) d\theta \\ & - 2 \operatorname{Re} \left(\int_0^\pi S^H X^H A B w(\theta) d\theta \right) \\ & + \int_0^\pi S^H A^H A S w(\theta) d\theta, \end{aligned} \quad (14)$$

where the superscript H denotes the Hermitian transpose. Using the orthogonality of the Legendre polynomials in Eq. (2), Eq. (14) reduces to

$$\chi^2 = B^H C B - 2 \operatorname{Re}(S^H D B) + S^H E S, \quad (15)$$

where a typical element of the matrix C is

$$C_{ij} = \frac{\pi R^2}{\rho c} \sum_{n=0}^{\infty} \Gamma_n^*(R) \Gamma_n(R) \frac{2}{2n+1} \mathbf{P}_n(\alpha_i) \mathbf{P}_n(\alpha_j), \quad (16)$$

and elements of D and E are similar in form. By differentiating the cost function with respect to each of the control forces f_i and setting all the differentials to zero, it is possible to show that the vector of control forces B_{opt} which minimizes the cost function is the solution to the normal equation

$$C B_{\text{opt}} = S^T D. \quad (17)$$

2. Obtaining the normal equations from discrete variables

Now suppose that the transfer functions are defined only at discrete locations \mathbf{r}_m , $m=1,2,\dots,M$, where \mathbf{r}_m is a location vector denoting a location in the far field. (This will always be the case with the numerical solution, and the analytical solution can also be used to generate values at discrete locations.) The form of X is

$$X = \begin{bmatrix} X_1(\mathbf{r}_1) & X_2(\mathbf{r}_1) & \cdots & X_N(\mathbf{r}_1) \\ X_1(\mathbf{r}_2) & X_2(\mathbf{r}_2) & \cdots & X_N(\mathbf{r}_2) \\ \vdots & \vdots & & \vdots \\ X_1(\mathbf{r}_M) & X_2(\mathbf{r}_M) & \cdots & X_N(\mathbf{r}_M) \end{bmatrix} \quad (18)$$

and likewise for A . Summing contributions to the cost function at each far-field location θ_m essentially performs a numerical integration of Eq. (6); thus it is possible to evaluate the coefficients of the normal equations and solve for the required control forces. For the numerically computed cost function to closely approximate the radiated power, two conditions must be satisfied. First, there must be enough far-field locations to adequately characterize the response. Second, the weighting function $w(\theta)$ must be discretized to account for the contributions of each location. This is accomplished by defining a diagonal matrix W in which each entry on the diagonal represents a different far-field location. Using the notation of the previous section, the C , D , and E matrices become

$$\begin{aligned} C &= X^H W X, \\ D &= A^H W X, \\ E &= A^H W A, \end{aligned} \quad (19)$$

and the normal equations are identical to Eq. (13).

If the total response is axisymmetric, then X and A contain acoustic pressures at far-field locations θ_m , $m=1,2,\dots,M_\theta$ (all at a constant value of ϕ). The row vectors X and B become matrices of column dimension M_θ . For example,

$$X = \begin{bmatrix} X_1(\theta_1) & X_2(\theta_1) & \cdots & X_N(\theta_1) \\ X_1(\theta_2) & X_2(\theta_2) & \cdots & X_N(\theta_2) \\ \vdots & \vdots & & \vdots \\ X_1(\theta_{M_\theta}) & X_2(\theta_{M_\theta}) & \cdots & X_N(\theta_{M_\theta}) \end{bmatrix}. \quad (20)$$

The entries in the diagonal weighting matrix W are weighting coefficients w_i proportional to the areas associated with each of the far-field locations. If the far-field locations are evenly spaced at intervals of $2\Delta\theta$, then

$$w_i = \begin{cases} \frac{\pi R^2}{\rho c} (1 - \cos \Delta\theta), & i=1 \text{ or } i=M_\theta \\ \frac{\pi R^2}{\rho c} [\cos(\theta_i - \Delta\theta) - \cos(\theta_i + \Delta\theta)], & 1 < i < M_\theta. \end{cases} \quad (21)$$

If the total response exhibits a plane of symmetry, then the variables must be partitioned to contain far-field pressures at θ_m , $m=1,2,\dots,M_\theta$ for each of the longitudinal locations ϕ_i , $i=1,2,\dots,M_\phi$. Thus the row vectors X and A become matrices whose column dimension is the product of M_θ and M_ϕ . The entries in the weighting matrix W must be similarly partitioned, and scaled proportional to the areas associated with each of the far-field locations. If the far-field locations are evenly spaced at intervals of $2\Delta\theta$ in the latitudinal direction and $\Delta\phi$ in the longitudinal direction, then the entries in W are the same as in Eq. (15) but divided by the number of intervals in the ϕ direction.

II. RESULTS AND DISCUSSION

The objectives of this section are (1) to show agreement between the analytical and numerical results, and (2) to discuss results of efforts to control radiation from a point-force disturbance.

The material properties and geometric specifications used for both the analytical and numerical models are summarized below. The model represents an undamped steel shell submerged in water. The shell material has Young's modulus of 1.85×10^{11} Pa, Poisson's ratio of 0.3, and density of 7670 kg/m^3 . The shell radius a is 1.0 m, and the wall thickness is 0.01 m. The density and acoustic velocity of the surrounding fluid are 1000 kg/m^3 and 1460 m/s , respectively. All far-field quantities are normalized to a distance of 1.0 m.

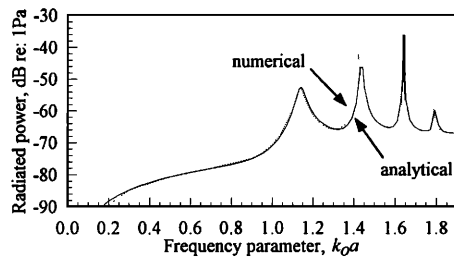


FIG. 2. Comparison of radiated power computed with analytical and numerical (NASHUA) solutions. Frequency regime $0 < k_0 a < 1.7$ contains three peaks; agreement is good between analytical and numerical results. Some frequency shifting occurs at higher frequencies.

A. Analytical and numerical predictions of disturbance response

Figure 2 compares the radiated power spectra obtained using the analytical and numerical models. The response contains sharp peaks at $k_0 a = 1.14, 1.44, 1.64,$ and 1.8 , the nature of which are detailed below. The two methods agree well in terms of magnitudes and overall trends, as could be expected for this simple structure. At frequencies above $k_0 a > 1.7$, the peaks in the numerical model are shifted to slightly lower frequencies. Reasons for this shift could include both modeling simplifications in the analytical solution and discretization approximations in the numerical model. For the purposes of this study, the region below $k_0 a = 1.7$ contains sufficient features that higher frequencies need not be treated here.

One difference between the analytical and numerical solutions appears in Fig. 3, which shows the distribution of surface velocity at a frequency of $k_0 a = 1.14$ due to a point-force disturbance without control. The two solutions agree well except near $\theta = 0^\circ$, the location at which the force is applied. The numerical solution, which accounts for bending as well as membrane stresses, displays large local deformations near the drive-point location; the analytical solution, which truncates high-order terms and does not account for bending stresses, does not exhibit local deformations. Fortunately, such short-wavelength disturbances do not propagate efficiently to the far field and can be ignored without affecting controller performance. When analytical and numerical velocity distributions are compared to check solution accuracy, one must expect such differences to occur near drive points.

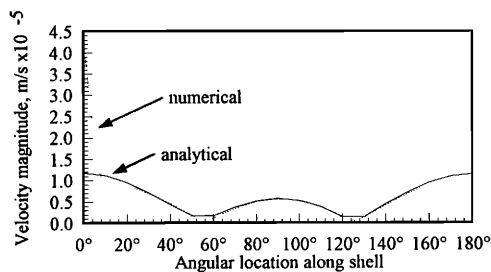
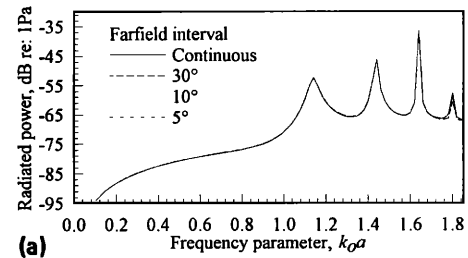
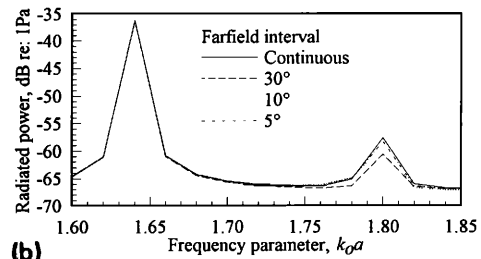


FIG. 3. Sample surface velocity distributions from analytical and numerical solutions ($k_0 a = 1.14$). Large local deformations near drive point occur in numerical solution but not analytical solution.



(a)



(b)

FIG. 4. Effect of far-field discretization on accuracy of radiated power calculations. Solid line represents continuous variables; other lines represent discretized variables with various mesh sizes. (a) Shows entire frequency range; (b) enlarges upper frequencies to show detail. At these low frequencies, 10° far-field interval is sufficient to capture dynamic response.

The solution accuracy also depends on the far-field interval $\Delta\theta$ used to compute radiated power, so it is necessary to verify that the choice of $\Delta\theta$ is sufficiently small to characterize the far-field behavior. (Recall that far-field locations are separated by an angle $2\Delta\theta$.) Since the analytical solution can use either continuous or discrete variables, the radiated power found using continuous variables can be compared to that found using discrete variables with different values of $\Delta\theta$. A small value of $\Delta\theta$ should provide the same radiated power found using continuous variables, and the agreement should deteriorate as $\Delta\theta$ increases. Figure 4(a) and (b) compare the radiated power spectra for continuous variables to that found using far-field intervals of $\Delta\theta = 2.5^\circ, 5^\circ,$ and 15° . Figure 4(a) shows the frequency range $0 < k_0 a < 1.9$, and Fig. 4(b) shows an enlarged view of the frequency range $1.6 < k_0 a < 1.9$. With $\Delta\theta = 2.5^\circ$ and 5° , the agreement with the continuous solution is excellent at all frequencies. Even with $\Delta\theta = 15^\circ$ the solution is adequate through $k_0 a = 1.7$. Results in this paper use a far-field interval of $\Delta\theta = 5^\circ$ to decrease computation times.

Figure 5 shows the shapes of the first few vibrational modes, denoted by the number n of nodal circles present. The curves shown are surface velocity distributions obtained using only the n th term from the summation in Eq. (2), and are normalized to unit maxima. The $n = 0$ mode is a “breathing” mode, i.e., a uniform radial expansion contraction. The $n = 1$ mode is a rigid-body translation, $n = 2$ is the first axial mode, and so forth. Each of the modes has an axis of symmetry corresponding to a diameter of the sphere (except for $n = 0$ which displays spherical symmetry). For $n > 0$ the modes are degenerate because there are infinitely many axes about which different modes occur. For example, the $n = 2$ mode that is symmetric about the $\alpha = 0^\circ$ diameter is *different*

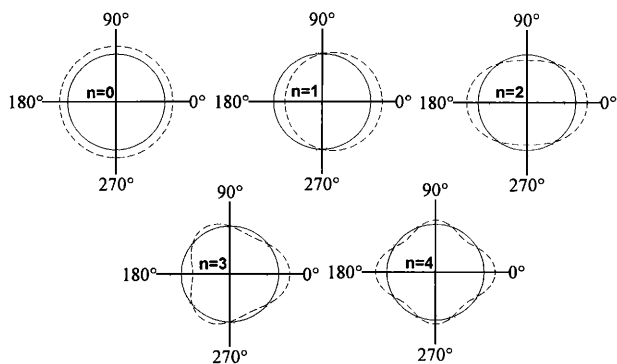


FIG. 5. Mode shapes of first few vibrational modes of the spherical shell, denoted by the number n of nodal circles present.

from the $n=2$ mode that is symmetric about the $\alpha=45^\circ$ diameter (although they occur at the same frequency). On the other hand, the $n=2$ mode that is symmetric about the $\alpha=0^\circ$ diameter is *identical* to the $n=2$ mode that is symmetric about the $\alpha=180^\circ$ diameter. This distinction is important to the discussion given in the next section, because modes that are excited by a point force at $\alpha=0^\circ$ are identical to those that are excited by a point force at $\alpha=180^\circ$.

Figure 6 shows the contributions of individual modes to the radiated power for a single point-force excitation. The modes are orthogonal and are not coupled by the presence of the fluid, so there are no cross terms in the radiated power. Because of high radiation damping, the $n=0$ mode does not display a separate peak in this frequency range, although it does contribute at all frequencies. The $n=1$ mode dominates the radiated power at very low frequencies, which can be considered the “resonant frequency” of the rigid-body mode. The $n=2, 3,$ and 4 modes each dominate the response at the frequencies $k_0 a = 1.14, 1.44,$ and 1.64 , respectively. These modal contributions are used below to help explain controller performance in terms of modal spillover.

B. ASAC using a single point force

To see whether a single control force can produce significant *global* attenuation, i.e., attenuation throughout the entire radiated field rather than in a localized area, examine how the presence of the control force affects the total radiated power. Figure 7 shows the radiated power spectra due to a unit-magnitude disturbance force at $\alpha=0^\circ$, before and after adding a single control force at $\alpha=180^\circ$ (numerical solu-

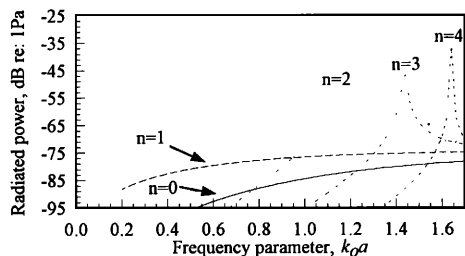


FIG. 6. Modal contributions to radiated power spectrum. The $n=0$ mode does not cause a separate peak in the response because of high radiation damping.

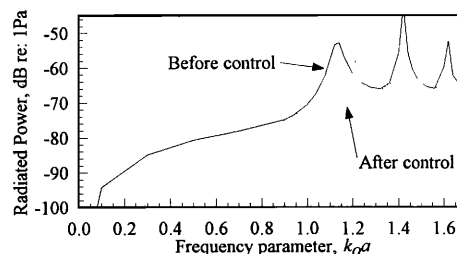


FIG. 7. Radiated power spectrum before and after applying a single control force at $\alpha=180^\circ$. Reductions of up to 20 dB are seen at resonance frequencies and at very low frequencies. Between resonances, little or no attenuation is seen.

tion). The control force reduces the radiated power by up to 20 dB at resonance frequencies and at very low frequencies; between resonances the reductions are smaller. There exist several frequencies at which there is no attenuation, a phenomenon that is explored later in this section.

Figure 8(a) compares the analytical and numerical solutions for the residual radiated power, that is, the radiated power after the control force has been added. The agreement between the two solutions is excellent, with discrepancies of less than 0.5 dB at frequencies below $k_0 a = 1.4$. At higher frequencies the levels agree quite well, but exhibit a slight frequency shift consistent with the frequency shift seen in Fig. 2 for the uncontrolled case.

Figure 8(b) compares the analytical and numerical solutions for the control force as a function of frequency. The force varies between $+1$ and -1 for a unit disturbance force; the largest control forces are required at resonance frequencies. Between resonances, the control force drops to zero at frequencies for which there is no reduction in radiated power. The numerical and analytical results agree very closely in levels, although they exhibit the same frequency shift seen in Figs. 2 and 8(a).

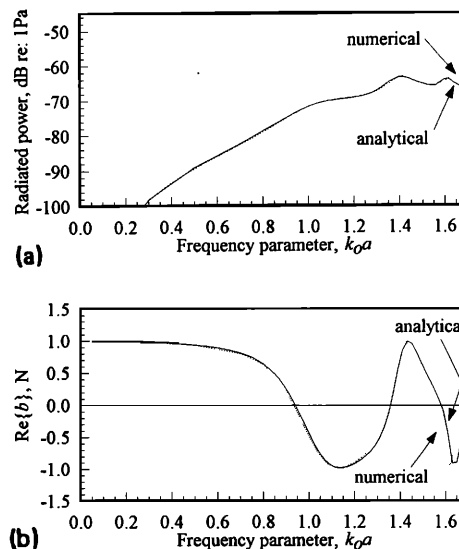


FIG. 8. Comparison of numerical and analytical solutions for (a) radiated power residual vs frequency, and (b) control force. Levels agree well between numerical and analytical solutions; slight frequency shift is observed at higher frequencies. For disturbance force of unit magnitude, control force varies between $+1$ and -1 with extrema occurring at resonance frequencies.

System dynamics can be illustrated by examining the modal components of the radiated power. Recall that the disturbance and control forces are arranged with a spatial separation of 180° , i.e., they act along the same diameter but at opposite poles of the shell. Referring to the earlier discussion of degenerate modes, if equal forces were applied at the disturbance and control locations, they would excite the same modes with the same relative magnitudes. There would, of course, be phase differences as a result of the spatial separation between the two forces. Contributions to even-numbered modes would be in phase with each other, while contributions to odd-numbered modes would be 180° out of phase. Two consequences must be considered in evaluating control performance. First, since all the disturbance modes are either in phase or out of phase with modes excited by the disturbance, the control force will always be purely real for a real disturbance force. Second, if the control force equals the disturbance force, some modal contributions from the disturbance force would be *doubled* in strength by the control force (even-numbered modes) while others would be *cancelled* (odd-numbered modes). If the control force attempted to eliminate the dominant mode, response in other modes could be increased by this “modal spillover.”

The column charts in Fig. 9(a)–(c) show the modal contributions to radiated power for $k_0a=1.14$, 0.94 , and 1.32 , respectively, before and after adding the control force. In Fig. 9(a), the disturbance response is clearly dominated by the $n=2$ mode. The control force, which is out of phase with the disturbance, eliminates the contributions of the $n=2$ mode and, by coincidence, the $n=0$ mode. The response is reduced everywhere both in the far field and on the structure itself, behavior that is often termed “modal suppression” because the dominant radiating mode is cancelled.⁷ However, the contributions from the $n=1$ and $n=3$ modes increase by 6 dB. The overall is thus limited because of spillover into modes that happen to be in phase with the control force.

In Fig. 9(b), the frequency is such that the disturbance response contains equal radiated power contributions from the $n=1$ and $n=2$ modes. If the control force attempts to cancel the $n=1$ mode, there is enough spillover into the $n=2$ mode that no net reduction in radiated power takes place. Similarly, the control force cannot achieve net improvements by attempting to cancel the $n=2$ mode. Any nonzero control force only increases the total radiated power, so the optimum solution is to set the control force to zero. Similar situations exist at every frequency for which there is no reduction in radiated power (Fig. 7) and, correspondingly, every frequency for which the control force magnitude is zero [Fig. 8(b)].

In Fig. 9(c) both the $n=2$ and $n=3$ modes contribute, but the larger contribution comes from the $n=2$ mode. The control force partially cancels the $n=2$ mode, but not beyond the balancing point at which spillover into uncontrolled modes would increase the radiated power. The net decrease in radiated power is 3 dB. Interestingly, although the radiated power is reduced, the vibration levels on the shell actually increase slightly. Figure 10 shows the numerically computed surface velocity distribution before and after applying the control force. As in Fig. 3, the solution exhibits relatively

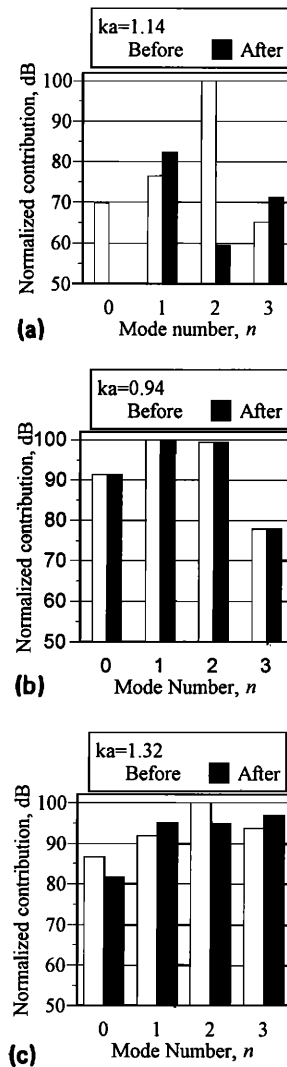


FIG. 9. Modal components of radiated power before and after applying control for (a) $k_0a=1.14$, (b) $k_0a=0.94$, (c) and $k_0a=1.32$. (a) Exhibits modal suppression; the $n=0$ and $n=2$ modes are reduced by 40 dB or more, but the $n=1$ and $n=3$ modes are boosted 6 dB by modal spillover. In (b) no reduction is possible with one control force. In (c) energy is transferred from $n=2$ mode to the less-efficient $n=3$ mode.

large local deformations near the drive points at 0° and 180° . Away from these regions, the surface velocity is actually higher after the control is applied even though the radiated power has decreased. This is similar to “modal restructuring,” in which the modal contributions are relatively un-

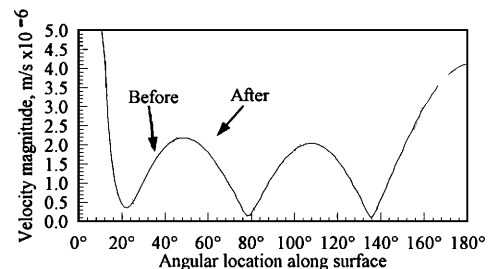


FIG. 10. Surface velocity magnitude before and after applying control force, $k_0a=1.32$. Energy is shifted from $n=2$ mode to less-efficient $n=3$ mode to decrease radiated power, but vibration levels actually increase.

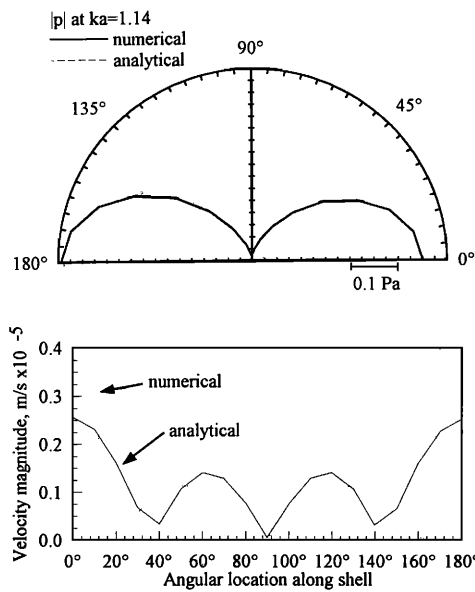


FIG. 11. Comparison of residual response found with analytical vs numerical methods at $k_0a=1.14$ (first resonance frequency). Solid line represents analytical results; the broken line represents numerical results. (a) Shows far-field pressure directivity; (b) shows surface velocity distribution. Far-field solutions agree extremely well. Local deformations near drive points in numerical solution do not propagate to far field, and thus do not affect control behavior.

changed in magnitude but their phases are rearranged to reduce radiation efficiency.⁷ In this case, however, energy is merely shifted from a mode that radiates efficiently into another mode with lower radiation efficiency. Modal restructuring cannot take place because the modes, being orthogonal radiators, cannot influence one another.

Numerical accuracy is reflected in part by the agreement between analytical and numerical methods in predicting the residual response, i.e., the response after the control force is applied. Because the controlled radiation levels are small, predicting residuals is often the most stringent test for numerical accuracy, particularly when the residual structural vibration may still be large. Figure 11(a) and (b) show the residual far-field pressure directivity and surface velocity distribution at $k_0a=1.14$, the same frequency examined in Fig. 9(a). Figure 12(a) and (b) show similar plots for $k_0a=1.32$, the same frequency examined in Fig. 9(c). In all cases, the numerical solution reproduces the analytical results to a satisfactory degree, with reasonable agreement on the general character of the residual if not on absolute levels. As seen in Fig. 3, the numerically computed surface velocities near the drive points exhibit significant local deformations that do not appear in the analytical solutions. However, these local surface deformations do not lead to acoustic propagation to the far field, as evidenced by the close agreement between numerically and analytically computed far-field pressure residuals. Overall, the small response levels encountered in predicting residuals do not appear to adversely affect the accuracy of the numerical approach.

C. ASAC using multiple forces

The results of the previous section imply that off-resonance frequencies require multiple control forces, since

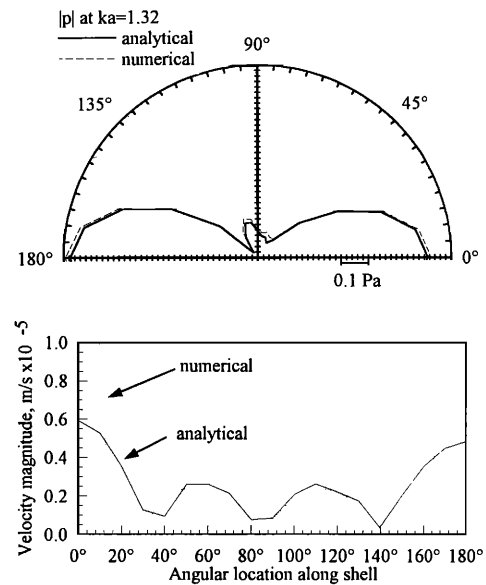


FIG. 12. Comparison of residual response found with analytical vs numerical methods at $k_0a=1.32$. Solid line represents analytical results; the broken line represents numerical results. (a) Shows far-field pressure directivity; (b) shows surface velocity distribution. Far-field solutions agree extremely well. Local deformations near drive points in numerical solution do not propagate to far field, and thus do not affect control behavior.

multiple modes contribute to the radiation. This inference is supported by Fig. 13, which shows numerical predictions of the system performance with multiple actuators. The solid line represents the disturbance response; the other lines represent the controlled response with one, two, four, and seven control forces. Each configuration has one control force at $\alpha=180^\circ$. The configurations with two, four, and seven forces also have control forces evenly spaced at intervals of 90° , 35° , and 25° respectively. Controller performance increases markedly as more control forces are added. This is especially true at off-resonance frequencies where multiple modes are present and thus multiple forces are required to control the radiation. Four control forces can achieve roughly 10 dB attenuation at $k_0a=0.94$, where a single actuator achieves no attenuation. Increasing the number of control forces to seven gives attenuations of 6 dB or more throughout the entire frequency range.

It should be noted here that no attempt has been made to

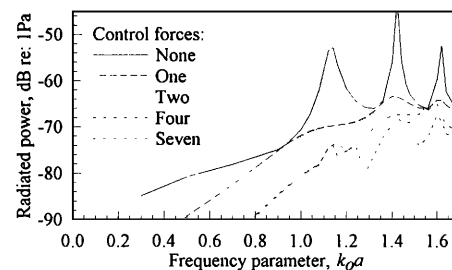


FIG. 13. Radiated power spectrum with multiple control forces. Solid line represents response with no control. Other lines represent response with one, two, four, and seven control forces. Increasing number of control forces improves performance, especially between resonances where multiple modes contribute to the response.

optimize the locations of the control forces. Similar reductions could likely be obtained with a smaller number of optimally placed control forces. The number of control forces needed could be as low as one control force per contributing mode, if control force locations were optimized so that each force could control a separate mode with no spillover into other modes.

III. SUMMARY

The primary research goal is to develop a computer program for investigating active structural-acoustic control (ASAC) of three-dimensional, fluid-loaded structures, and check its performance by investigating an example structure. For generality, a numerical approach is used to calculate structural-acoustic dynamic responses. The feedforward control approach used is based on minimizing the radiated power at a single frequency. The example structure chosen is a thin-walled, fluid-loaded, spherical shell, and numerical results are compared to an analytical solution.

The analytical and numerical models for the spherical shell agree well both in response characterizations and in solutions to the active control problem. Numerical and analytical solutions for the uncontrolled response display excellent agreement below $k_0a=1.4$, with some frequency shifting in the region $1.4 < k_0a < 1.7$. Predictions of controller performance, including control forces and reductions of radiated power, agree well but are subject to the same frequency shift. Short-wavelength structural responses that appear in the numerical solution but not the analytical solution do not affect the far-field behavior, and therefore do not affect the controller performance. Numerical predictions of residual responses agree with analytical predictions to the same extent that uncontrolled predictions agree. In general, the results give confidence that the methods described could be used to examine other, more complicated structures for which no analytical models exist.

For the spherical shell, ASAC is an efficient method for controlling radiated noise at low frequencies ($0 < k_0a < 1.7$). At resonance frequencies, radiation due to a point-force disturbance can be reduced by up to 20 dB using only one actuator. The mechanism for reducing radiated power on-resonance is modal suppression, in which the dominant response mode is completely suppressed. Between resonances, multiple actuators are required to obtain large reductions.

The main mechanism for reducing radiated power off-resonance is that energy is transferred to less-efficient modes, which can actually increase vibration levels. Increasing the number of control forces improves controller performance. With seven control forces, attenuations of at least 6 dB can be obtained over the entire frequency range $0 < k_0a < 1.7$.

ACKNOWLEDGMENTS

This project is part of a doctoral program made possible by the Extended-Term Training Program at the Carderock Division, Naval Surface Warfare Center. The work has also been funded by the Office of Naval Research through Grant No. ONR-N00014-92-J-1170.

- ¹C. R. Fuller, "Apparatus and method for global noise reduction," US Patent No. 4,715,599 (1987).
- ²C. R. Fuller, "Active control of sound transmission/radiation from elastic plates by vibration inputs: I. Analysis," *J. Sound Vib.* **136**, 1–15 (1990).
- ³C. R. Fuller and J. D. Jones, "Experiments on reduction of propeller-induced interior noise by active control of cylinder vibration," *J. Sound Vib.* **112**, 389–395 (1987).
- ⁴C. Guigou and C. R. Fuller, "Active control of sound radiation from a simply supported beam: Influence of bending near-field waves," *J. Acoust. Soc. Am.* **93**, 2716–2725 (1993).
- ⁵R. Clark and C. R. Fuller, "Control of sound radiation with adaptive structures," *J. Intelligent Mater. Syst. Struct.* **2**, 431–452 (1991).
- ⁶Y. Gu and C. R. Fuller, "Active control of sound radiation due to subsonic wave scattering from discontinuities on fluid-loaded plates. I: Far-field pressure," *J. Acoust. Soc. Am.* **90**, 2020–2026 (1991).
- ⁷C. R. Fuller, C. H. Hansen, and S. D. Snyder, "Active control of sound radiation from a vibrating rectangular panel by sound sources and vibration inputs: An experimental comparison," *J. Sound Vib.* **145**, 195–215 (1991).
- ⁸G. C. Everstine and A. J. Quezon, "User's guide to the coupled NASTRAN/Helmholtz equation capability (NASHUA) for acoustic radiation and scattering," CDNSWC-SD-92-17, Carderock Division, NSWC, Bethesda, MD (1992).
- ⁹C. G. Molo and R. J. Bernhard, "Generalized method of predicting optimal performance of active noise controllers," *AIAA J.* **27**, 1473–78 (1989).
- ¹⁰K. A. Cunefare and G. H. Koopmann, "A boundary element approach to optimization of active noise control sources on three-dimensional structures," *Trans. ASME J. Vib. Acoust.* **113**, 387–394 (1991).
- ¹¹C. E. Ruckman and C. R. Fuller, "Numerical simulation of active structural-acoustic control for a fluid-loaded spherical shell," Proceedings of the Second International Congress on Recent Developments in Air- and Structure-Borne Sound and Vibration, Auburn University, 1992, edited by M. J. Crocker and P. K. Raju (unpublished), pp. 377–385.
- ¹²M. C. Junger and D. Feit, *Sound, Structures, and Their Interaction* (MIT, Cambridge, 1986), 2nd ed.